BNL-222531-2021-JAAM

Solvated Electron in Acetonitrile: Radiation Yield, Absorption Spectrum, and Equilibrium Between Cavity- and Solvent-Localized States

D. C. Grills

To be published in "The Journal of Physical Chemistry B"

December 2021

Chemistry Department

Brookhaven National Laboratory

U.S. Department of Energy

USDOE Office of Science (SC), Basic Energy Sciences (BES) (SC-22)

DISCLAIMER

Solvated Electron in Acetonitrile: Radiation Yield, Absorption Spectrum, and Equilibrium Between Cavity- and Solvent-Localized States

David C. Grills and Sergei V. Lymar**

Chemistry Division, Brookhaven National Laboratory, Upton, NY 11973-5000, United States

AUTHOR INFORMATION

Corresponding Authors

*Email: dcgrills@bnl.gov

*Email: lymar@bnl.gov

ABSTRACT: The equilibrium between a solvent cavity-localized electron, e^-_{cav}, and a dimeric solvent anion, $(CH_3CN)_2^{\bullet-}$, which are the two lowest energy states of the solvated electron in acetonitrile, has been investigated by pulse radiolysis at 233-353 K. The enthalpy and entropy for the e^-_{cav} to $(CH_3CN)_2^{\bullet-}$ conversion amount to –11.2 ± 0.3 kcal/mol and –39.3 ± 1.2 cal/(mol K), corresponding to a 0.44 ± 0.35 equilibrium constant at 25 °C. The radiation yield of the solvated electron has been quantified using a Co(II) macrocycle that scavenges electrons with a 1.55×10^{11} M^{-1} s^{-1} rate constant. The apparent yield increases without saturation over the attainable scavenger concentration range, reaching 2.8 per 100 eV; this value represents the lower limit for the acetonitrile ionization yield in pulse radiolysis. The apparent molar absorption coefficient of (20.8 ± 1.5) × 10^3 M^{-1} cm^{-1} at 1450 nm and 20 °C for the solvated electron, and individual Vis-NIR absorption spectra of e^-_{cav} and $(CH_3CN)_2^{\bullet-}$, are derived from the data. Variances with previous reports are thoroughly discussed. Collectively, these results resolve several controversies concerning the solvated electron properties in acetonitrile and furnish requisite data for quantitative pulse radiolysis investigations in this commonly used solvent.

INTRODUCTION

As a polar, nearly aprotic solvent with excellent solubilizing ability, moderate nucleophilicity, and large electrochemical and optical transparency windows, acetonitrile (CH_3CN) is an extensively used medium for investigating redox reactions by various time-resolved techniques. Among those, pulse radiolysis is of particular utility, for it allows rapid solvent ionization with attendant generation of solvated electrons. Scavenging of these electrons by solutes has been used for initiating a variety of reductive chemistries.[e.g., 1-13] Requisite for quantitative interpretation of such studies are the radiation chemical yield, properties, and reactivity of the solvated electron, which is the subject matter of this work. Here, we will use the term "solvated electron" collectively for all reducing species that result from energy stabilization of a thermalized quasi-free (conduction band) electron in liquid CH_3CN, regardless of their structures and types of electron-solvent interactions involved in the stabilization. The term "excess electron" is also used in the literature in the same sense, but we find this term to be somewhat less descriptive and overly inclusive, for it does not discriminate between the conduction and valence band electrons.

In their seminal 1977 pulse radiolysis study, Rodgers and co-workers discovered that in 60 °C CH_3CN, the radiolytically-generated solvated electron exhibits a wide and strong NIR absorption band centered at 1450 nm, whose amplitude monotonically decreases upon sample cooling to –40 °C with concomitant growth of a much weaker visible band around 500 nm.[5] This highly unusual behavior was attributed to the existence of an equilibrium between two states that are accessible to the solvated electron in liquid CH_3CN, one being a solvent anion radical, $CH_3CN^{\bullet-}$, and the other a dimeric solvent anion (dsa) radical, $(CH_3CN)_2^{\bullet-}$, containing two solvent molecules; that is, $CH_3CN^{\bullet-} + CH_3CN \rightleftharpoons (CH_3CN)_2^{\bullet-}$. Further, it was suggested that the monomer and dimer anion radicals are responsible for the 1450 nm and 500 nm bands, respectively, and that their

equilibration occurs much faster than 20 ns. Although no value for the equilibrium constant was derived from the data, the enthalpy of dimerization was estimated as −8.34 kcal/mol.

A quarter century later, the nature of the solvated electron in CH_3CN was further clarified by laser flash photolysis studies. Using pump-probe spectroscopy and deriving the solvated electron from photoionization of iodide or indole,[14] Kohler and co-workers confirmed the existence of both strong NIR and weaker visible absorption bands consistent with those reported by Rodgers and co-workers and attributable to two different solvated electron states that equilibrate with a time constant of ~0.26 ns. Simultaneously, Shkrob and Sauer used time-resolved dc conductivity to observe two kinds of electron photoejected from benzene dissolved in CH_3CN that are distinguishable by their mobility and reactivity.[15] However, their equilibration time estimate of ~3 ns is about 10 times larger than that of Kohler and co-workers. Both these reports concur with Rodgers and co-workers' suggestion of $(CH_3CN)_2^{\bullet-}$ being the low-temperature state of the solvated electron, but present experimental and/or electronic structure computational evidence against the assignment of the high-temperature NIR absorbing species to the $CH_3CN^{\bullet-}$ anion. Instead, this species is suggested to be structurally analogous to a familiar cavity electron (e^-_{cav}) bound to the surrounding solvent molecules by ion-dipole interactions, which is believed to be the predominant form of solvated electron in water, alcohols, and several other polar solvents.[16] Additionally, experimental[17-20] and theoretical[17, 21-25] investigations of $(CH_3CN)_n^-$ clusters, particularly recent *ab initio* molecular dynamics simulations,[26] have also provided compelling evidence for two solvated electron states in CH_3CN, namely e^-_{cav} and $(CH_3CN)_2^{\bullet-}$. Thus, the equilibrium between the two solvated electron states is better described as,

$$e^-_{cav} + 2CH_3CN_{liq} \rightleftharpoons (CH_3CN)_2^{\bullet-} \qquad (1)$$

and its standard equilibrium constant is,

$$K^{o} = \frac{[(CH_3CN)_2^{\bullet -}]}{[e^-_{cav}]} = exp\left(-\frac{\Delta G^{o}}{RT}\right) = exp\left(-\frac{\Delta H^{o}}{RT} + \frac{\Delta S^{o}}{R}\right) \quad (2)$$

where $\Delta G°$, $\Delta H°$, and $\Delta S°$ are the standard Gibbs free energy, enthalpy, and entropy of reaction 1, respectively.[27] The equilibrium distribution between the two states is given by,

$$[e^-_{cav}] = [e^-_{solv}]\frac{1}{1+K^{o}} \quad \text{and} \quad [(CH_3CN)_2^{\bullet -}] = [e^-_{solv}]\frac{K^{o}}{1+K^{o}} \quad (3)$$

where $[e^-_{solv}] = [e^-_{cav}] + [(CH_3CN)_2^{\bullet -}]$ is the total solvated electron concentration. From a rather involved data analysis, Shkrob and Sauer evaluated $\Delta H° = -10.6 \pm 0.9$ kcal/mol and $K^{o} = 1.32 \pm 0.2$ at 25 °C; the latter value implies only slight preference for the $(CH_3CN)_2^{\bullet -}$ solvated electron state at or near room temperature.

More recently, Doan and Schwartz expanded the aforementioned investigation of iodide photoionization in CH_3CN using a more sophisticated pump-probe spectroscopic technique.[28-29] Although they generally concurred with the two-state solvated electron model and its formulation given by reaction 1, a much shorter equilibration time of only 0.08 ns was derived from the data, which was attributed to CH_3CN contamination by water in the prior studies. Moreover, the "room temperature" $K°$ value was revised to 4.1 ± 0.2,[28] and it was concluded that solvated electrons favor the $(CH_3CN)_2^{\bullet -}$ state over the e^-_{cav} state.

As with the quantitative data on equilibrium between e^-_{cav} and $(CH_3CN)_2^{\bullet -}$, values of the radiation chemical yield (Table S1) of the solvated electron[2-3, 5, 8, 30] and the absorption spectra of its two forms[1, 5, 14, 28-29] that have been reported by several groups over the years, differ substantially. In the hope to clarify these controversies, we have re-investigated the temperature dependence of equilibrium 1 following pulse radiolysis of neat CH_3CN, which has resulted in a revision of the previously reported $K°$ values. We also show that the use of a cobalt-based macrocyclic complex as a solvated electron scavenger allows an accurate quantification of its radiation yield and

apparent molar absorption coefficient, both of which are found to differ from the previously reported values. From a practical standpoint, these new data allow direct quantitative evaluation of the total solvated electron concentrations in pulse radiolysis or flash photolysis studies.

EXPERIMENTAL METHODS

Materials. CH_3CN (Sigma-Aldrich, HPLC Plus, ≥99.9%) was purified by refluxing over KBH_4 for several hours followed by distillation, freeze-pump-thaw degassing on a high-vacuum line, and vacuum-transfer onto activated 3Å molecular sieves, where the solvent was kept for several days prior to use for the sample preparations in a nitrogen-filled glovebox. The perchlorate salt of the Co(II) macrocycle (**CoL**$^{2+}$), *N*-*rac*-[Co(HMD)(H_2O)](ClO_4)$_2$, where HMD = 5,7,7,12,14,14-hexamethyl-1,4,8,11-tetraazacyclotetradeca-4,11-diene, was synthesized according to a literature procedure;[31] upon dissolution in CH_3CN, the axial H_2O ligand in this complex is replaced by CH_3CN.

Pulse Radiolysis. The majority of the pulse radiolysis experiments were carried out at the 9 MeV BNL Laser Electron Accelerator Facility,[32] using electron pulses that are less than 50 ps in duration and deliver ~2–3 krad/pulse radiation doses. The detection optical path consisted of a pulsed xenon arc lamp, a 0.5 cm long quartz optical cuvette with an airtight Teflon valve, a selectable 10 nm bandpass interference filter, and either a silicon or a germanium photodiode (2-3 ns response time). For variable temperature experiments, a home-built thermostat capable of sample temperature control to within ±0.5 °C was used.

The pulse radiolysis experiment on electron scavenging by **CoL**$^{2+}$ requiring higher dosimetry precision and pulse-to-pulse dose reproducibility (data in Figures 2b and 3 and Table S2) were carried out with 2 MeV electrons from a Van de Graaff accelerator using 60-400 ns near-

rectangular pulses delivering 0.3-1.7 krad/pulse radiation doses that generated 0.25-1.4 μM concentrations of solvent-derived radicals or ions per unit *G*-value (here and throughout, the radiation yields, *G*-values, are given in number of radicals or ions per 100 eV absorbed energy). All experiments were performed using a 2 cm long quartz cell in the detection optical path with temperature stabilization at 25 ± 0.5 ºC.

In both radiolysis systems, the radiation dosimetry was performed at room temperature in the same sample cells that were used for the data collection, but with an N_2O-saturated 10 mM KSCN aqueous solution, using $G\varepsilon = 4.87\times10^4$ ions $(100\ eV)^{-1}\ M^{-1}\ cm^{-1}$ for $(SCN)_2^{\bullet-}$ at 472 nm. Temperature-dependent solvent density corrections were made when applying this dosimetry to pulse radiolysis of the CH_3CN samples. Additional details of the pulse radiolysis experiments are provided in the SI Section 1.

Where possible, uncertainties are given as one standard deviation of multiple measurements.

RESULTS AND DISCUSSION

Equilibrium. To obtain the thermodynamic parameters of equilibrium 1, transient absorption kinetic traces have been recorded at 1450 nm following pulse radiolysis of neat N_2-purged CH_3CN at various temperatures from –40 to 80 °C. Although these experiments are analogous to those described by Rodgers and co-workers, we used much shorter electron pulses and a faster detector, allowing a more accurate representation of the data at early times, and extended the measurements to a higher temperature. The temperature dependencies of the initial absorption amplitude at 1450 nm (*A*, obtained as detailed in SI Section 2) of the equilibrated mixture of e^-_{cav} and $(CH_3CN)_2^{\bullet-}$ are plotted in Figure 1a for two different solvated electron concentrations that were modulated by

radiation doses. The sigmoid shape of these curves is consistent with that expected based on eqs 2 and 3, provided both $\Delta H°$ and $\Delta S°$ are negative,

$$A = \frac{A_{\max} + A_{\min} exp\left(-\frac{\Delta H^0}{RT} + \frac{\Delta S^0}{R}\right)}{1 + exp\left(-\frac{\Delta H^0}{RT} + \frac{\Delta S^0}{R}\right)} \quad (4)$$

Here, $A_{\max}$ and $A_{\min}$ are the asymptotic high- and low-temperature absorption amplitudes, when all solvated electrons occupy their cavity and dimeric solvent anion states, respectively. Thus, for a unity optical path and fixed radiation dose, $A_{\max} = \varepsilon_{cav}[e^-_{solv}]$ and $A_{\min} = \varepsilon_{dsa}[e^-_{solv}]$, where ε_{cav} and ε_{dsa} are the respective molar absorption coefficients of the cavity electron and dimeric solvent anion.

It is clear from Figure 1a that the lowest and highest temperature data points must be close to the corresponding $A_{\min}$ and $A_{\max}$ asymptotic values, which means that equilibrium 1 nearly entirely shifts from $(CH_3CN)_2^{\bullet-}$ to e^-_{cav} over the 120 degrees temperature range. This fact allows a crude but straightforward evaluation of $\Delta H°$ and $\Delta S°$. Assuming that 97 to 99 % of the solvated electrons are present as e^-_{cav} at 80 °C and as $(CH_3CN)_2^{\bullet-}$ at –40 °C, we estimate a –13 to –10 kcal/mol range for $\Delta H°$ and –45 to –34 cal/(mol K) for $\Delta S°$ (see SI Section 3). To refine these values and obtain their standard deviations, we have performed nonlinear, least-squares fits of two independently measured A vs T datasets to eq 4 as shown in Figure 1a and averaged the results. This procedure yields $\Delta H° = –11.2 \pm 0.3$ kcal/mol, $\Delta S° = –39.3 \pm 1.2$ cal/(mol K), and $A_{\max}/A_{\min} = 24.5 \pm 5.1$. Because allowable variation for each of these parameters is confined to a narrow region as shown by the crude estimate above and Figure 1b inset, we are confident that their fitted values correspond to the global minimum. The large value of the $A_{\max}/A_{\min}$ ratio indicates that the molar absorption coefficient of the dimeric solvent anion at 1450 nm is only ~4% of that for the cavity electron.

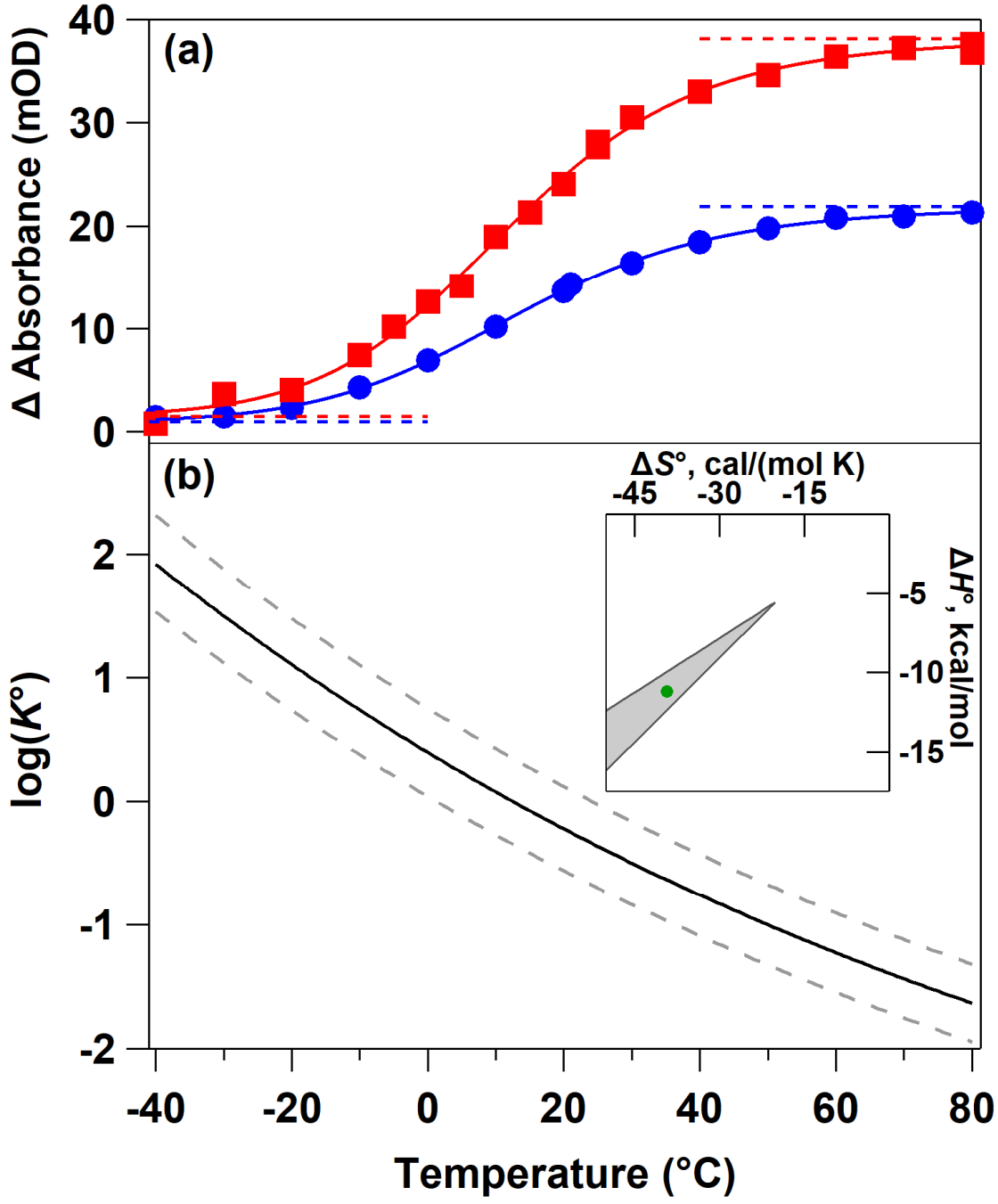

Figure 1. (a) Temperature dependencies of the initial absorption amplitude at 1450 nm for two different concentrations of the solvated electron (circles and squares) in N_2-purged CH_3CN. Curves show fits of the data sets to eq 4 with: A_{max} = 38.2 ± 0.5 mOD, A_{min} = 1.50 ± 0.55 mOD, $\Delta H°$ = –11.4 ± 0.6 kcal/mol, $\Delta S°$ = –40.1 ± 2.0 cal/(mol K) for squares, and A_{max} = 21.9 ± 0.3 mOD, A_{min} = 0.93 ± 0.15 mOD, $\Delta H°$ = –11.0 ± 0.3 kcal/mol, $\Delta S°$ = –38.4 ± 1.1 cal/(mol K) for circles. The

dashed lines mark the asymptotic A_{max} and A_{min} positions. (b) Temperature dependence of the equilibrium constant K^o computed using eq. 2 and the mean values of $\Delta H°$ and $\Delta S°$ from the two fits (solid line); dashed lines straddle the standard deviation for log($K°$). The inset shows the range of allowable ΔH^o and ΔS^o values (shaded cuneate area) for the equilibrium shift from >90 % predominance of the dimer solvent anion at –40 ºC to >90 % predominance of e^-_{cav} at 80 ºC (see SI section 3 for details), and the green dot corresponds to the ΔH^o and ΔS^o measured in this work.

The temperature dependence of the equilibrium constant for reaction 1 is plotted in Figure 1b. Over the entire temperature range, the value of $K°$ decreases by a factor of ~3700 and amounts to $K° = 0.60 \pm 0.49$ at 20 °C and 0.44 ± 0.35 at 25 °C. These values suggest that around room temperature, solvated electrons are nearly equally distributed between their cavity and dimeric solvent anion states, with only a slight preference for the former. The relatively large uncertainties in $K°$ arise from its power dependence on the $\Delta H°$ and $\Delta S°$ values, which greatly magnifies their comparatively small uncertainties. The steep temperature dependence of $K°$ is due to a large negative $\Delta S°$ arising from: (i) loss of translational entropy upon coalescence of three particles into one in reaction 1, and (ii) stronger charge localization with attendant tighter solvation in the solvent dimer anion state compared to the cavity electron state.

Comparing our and previously published thermochemical data for equilibrium 1, we note that our $\Delta H°$ is almost 3 kcal/mol more negative than –8.34 kcal/mol derived by Rodgers and co-workers from their absorbance vs temperature data through, what we find, a rather ambiguous procedure (see SI Section 4 for a detailed assessment). On the other hand, our enthalpy value lies within the error margins of $\Delta H° = -10.6 \pm 0.9$ kcal/mol obtained by Shkrob and Sauer from a temperature-dependent transient conductivity measurement. Our $K° = 0.44 \pm 0.35$ at 25 °C is nominally by a factor of 3 smaller than the Shkrob and Sauer value of 1.32 ± 0.2 for the same

temperature. However, we notice a mismatch between their stated uncertainties for $\Delta H°$ and $K°$. Indeed, their ±0.9 kcal/mol error in $\Delta H°$ by itself engenders a ±1.9 error in $K°$, which engulfs both their and our $K°$ values. The latest reported "room temperature" $K° = 4.1 \pm 0.2$ derived by Doan and Schwartz from time-dependent solvated electron spectra cannot be reconciled with our results. Later in this paper, we will show that this high $K°$, at least partially, arises from their use of a too low literature value of the e^-_{cav} molar absorption coefficient in their $K°$ derivation. The relatively high ionic strength arising from the 5 mM of tetrabutylammonium iodide used in that study might also have contributed to the $K°$ overestimate through ion paring between the tetrabutylammonium cation and the $(CH_3CN)_2^{\bullet -}$ anion, resulting in preferential stabilization of this solvated electron state. Finally, we note that ours and all other previously reported $\Delta H°$ values are difficult to reconcile with the large 24.4 kcal/mol separation of the two peaks at 2.61 and 3.67 eV in the photoelectron spectrum of the solvated electron in a CH_3CN microjet observed by Neumark and co-workers, which were attributed to e^-_{cav} and $(CH_3CN)_2^{\bullet -}$, respectively.[20] As detailed in SI Section 5, to make these data compatible with our directly measured $\Delta H°$ value, it is necessary to assume that bringing two CH_3CN solvent molecules together to the same geometry as in $(CH_3CN)_2^{\bullet -}$ requires ~13 kcal/mol more energy than arranging several CH_3CN solvent molecules into the same cavity geometry as in e^-_{cav}. Because the assumption of such a large energy difference appears to be unrealistic, we are tempted to suggest that at least one of the photoelectron peaks observed by Neumark and co-workers belongs to a surface rather than a bulk localized solvated electron state in the microjet.

Although rapid reversible attachment of the quasi-free (conduction band) electrons to solvent molecules has either been observed[33] or proposed as the first step of the quasi-free electron solvation in several solvents,[34, 16, 35] acetonitrile is presently the only solvent in which rapid

equilibrium between two metastable solvated electron states, that strongly shifts from one state to the other with temperature, has been detected. Moreover, we believe that the chances for observing an analogous solvated electron behavior in another solvent are rather slim. The main reason for this conjecture is that the values of $\Delta H°$ and $\Delta S°$ for an equilibrium shift between the two solvated electron states must be attuned in a manner specific to the liquid state temperature range of the solvent. This assertion is elaborated in SI Section 3 and illustrated in Figure 1b inset, which shows that the suitable $\Delta H°$ and $\Delta S°$ values for the observability of equilibrium 1 in CH_3CN must reside within a relatively small cuneate area on the $\Delta H°$-$\Delta S°$ surface, and that our measured $\Delta H°$ and $\Delta S°$ do belong in this area. In SI Figure S2, we show analogous $\Delta H°$-$\Delta S°$ diagrams for several other solvents in which metastable solvent radical anions have been observed: acetone, formamide, hexafluorobenzene, *N*-methylacetamide, pyrrolidone, benzene, and toluene.[16, 33] Notably, in none of these solvents has the coexistence of the solvent radical anions with cavity electrons or any other solvated electron state been detected. In addition to the restrictions on the allowable $\Delta H°$ and $\Delta S°$, to be observable, attachment of the cavity electron to a solvent molecule must not be dissociative, and its equilibration with a solvent anion must occur more rapidly than the overall solvated electrons decay through all pathways. Based on this discussion, we will not be surprised if CH_3CN turns out to be a unique solvent that serendipitously meets all the stringent requirements for examining the equilibrium between the two solvated electron states.

Electron scavenging and radiation yield. The radiation chemical yield of the solvated electron ($G(e^-_{solv}) = G(e^-_{cav}) + G((CH_3CN)_2^{\bullet -})$) has been quantified using a Co(II) complex with a macrocyclic ligand (**CoL**$^{2+}$; see structure in Scheme 1a) as an electron scavenger. In addition to its high solubility, **CoL**$^{2+}$ has several other desirable properties for this purpose: (i) it has been shown that one-electron reduction with Na(Hg) amalgam yields a **CoL**$^{+}$ product that persists in

dry, deoxygenated CH_3CN, allowing an accurate measurement of its absorption spectrum by conventional spectrophotometry,[36] which is the most important prerequisite for quantification of the solvated electron radiation yield using a scavenger, (ii) conveniently, the $\mathbf{CoL}^{+}$ species exhibits a strong characteristic absorption band (λ_{max} = 678 nm, ε_{max} = 18.0 × 10^3 M^{-1} cm^{-1}) in a region clear of the absorption by the CH_3CN solvent radiolysis products,[12] and (iii) being a divalent cation, $\mathbf{CoL}^{2+}$ is an extremely efficient solvated electron scavenger (vide infra).

As shown by the data in Figure 2a, addition of $\mathbf{CoL}^{2+}$ accelerates the e^-_{solv} decay, consistent with the reaction,

$$\mathbf{CoL}^{2+} + e^-_{solv} \longrightarrow \mathbf{CoL}^{+} \qquad k_5 \qquad (5)$$

The complex e^-_{solv} decay kinetics in neat CH_3CN becomes exponential upon addition of $\mathbf{CoL}^{2+}$ in excess over e^-_{solv}, and the observed pseudo first-order decay rate constants (k_{obs}) linearly increase with the $\mathbf{CoL}^{2+}$ content in the 0.05-0.23 mM range, which yields essentially diffusion-controlled k_5 = (1.55 ± 0.02) × 10^{11} M^{-1} s^{-1} (SI Figure S5a). This rate constant is ~3.5 times larger than the corresponding value in aqueous solution,[37] which is attributable to the lower viscosity of CH_3CN that increases the reactants' mobility and the greater dielectric constant of H_2O that decreases their coulombic attraction. Because both e^-_{cav} and $(CH_3CN)_2^{\bullet-}$ could contribute to $\mathbf{CoL}^{2+}$ reduction, and under the prevailing conditions equilibration between e^-_{cav} and $(CH_3CN)_2^{\bullet-}$ is much more rapid than reaction 5 (Scheme 1b), this rate constant represents a weighted average of the rate constants for reduction of $\mathbf{CoL}^{2+}$ by e^-_{cav} and $(CH_3CN)_2^{\bullet-}$; that is, $k_5 = (k_5' + k_5'' K^{o})/(1 + K^{o})$.

Scheme 1. (a) Structure of the CoL^{2+} (*N-rac*-[Co(HMD)]^2) electron scavenger, and (b) its solvated electron scavenging mechanism

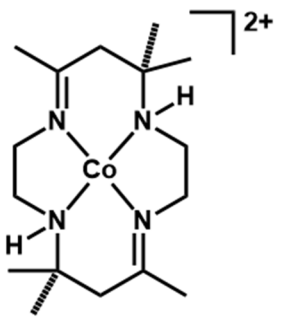

(a)

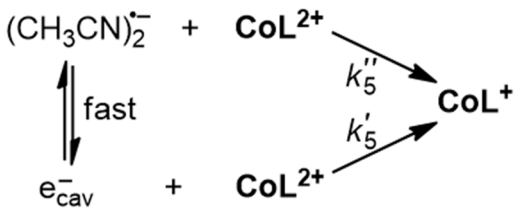

(b)

The formation of **CoL**$^{+}$ attributable to reaction 5 is readily detected by the rapid rise of transient absorption at or near its 678 nm band (Figures 2a, inset and 2b). To further verify that this absorption is due solely to reaction 5, Ar-purging has been replaced by saturation with N_2O, which is commonly used to convert solvated electrons into oxyl radical anions,

$$N_2O + e^-_{solv} \longrightarrow N_2 + O^{\bullet -} \qquad k_6 \qquad (6)$$

As a preliminary, the dependence of the e^-_{solv} decay rate upon N_2O partial pressure has been measured, which yielded $k_6 = (6.42 \pm 0.06) \times 10^9$ atm^{-1} s^{-1} (SI Figure S5b). Thus, in 1.28 mM **CoL**$^{2+}$ solutions under 1 atm of N_2O, the expected e^-_{solv} half-life is ~0.10 ns due to reactions 5 and 6, but less than 5% of e^-_{solv} would engage in the production of **CoL**$^{+}$. Accordingly, only negligible prompt transient absorption is observed under these conditions (Figure 2b, lower trace). Instead, a weak absorption develops and decays on the ~50 and ~500 μs timescales, respectively, and the kinetic trace can be satisfactorily fitted by a biexponential function. Although not further investigated, this pattern is consistent with the consecutive first- or pseudo first-order formation and decay of an intermediate originating from the oxyl radical anion.

As seen in Figure 2b, promptly radiolytically produced **CoL**$^{+}$ slowly decays via a second-order process, in contrast to chemically produced **CoL**$^{+}$, which is stable in dry, deoxygenated CH_3CN.[36]

Thus, the observed decay cannot be due to dimerization or disproportionation of $\mathbf{CoL}^+$. Most likely, $\mathbf{CoL}^+$ decays by recombination with the solvated protons to yield a hydride,

$$\mathbf{CoL}^+ + H^+_{solv} \longrightarrow \mathbf{CoL}(H)^{2+} \qquad (7)$$

We have previously shown that the $CH_3CN^{\bullet+}$ radical cation left behind by CH_3CN solvent ionization is a superacid acid ($pK_a \approx -45$ in CH_3CN) that extremely rapidly expels H^+_{solv}.[12] Thus, e^-_{solv} and H^+_{solv} are generated in the same quantities, hence the second order rate law for reaction 7. An analogous reaction occurring with a $(2–3) \times 10^9$ M^{-1} s^{-1} rate constant and leading to the disappearance of the characteristic $\mathbf{CoL}^+$ absorption spectrum has also been observed in aqueous solutions.[38, 37]

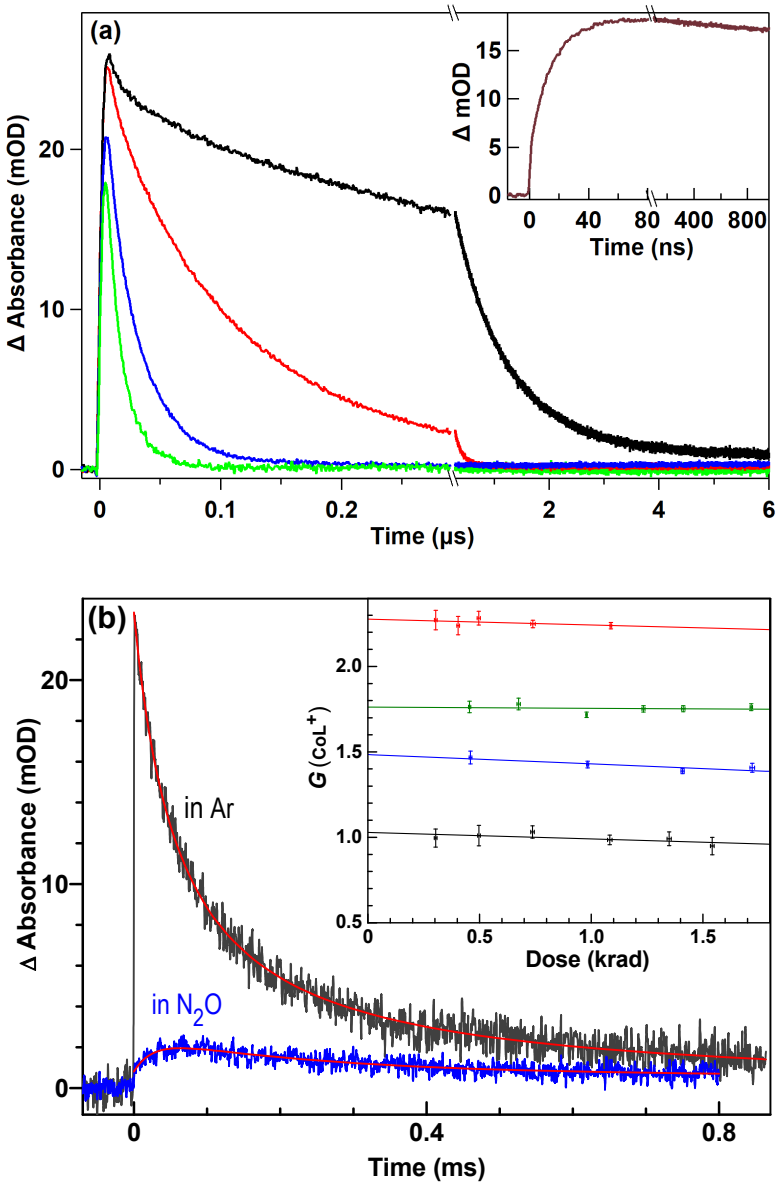

Figure 2. (a) Representative kinetic traces of e^-_{solv} formation and decay recorded at 1450 nm following pulse radiolysis of N_2-purged CH_3CN without (black) and with 49 (red), 228 (blue) and 503 (green) μM added $\mathbf{CoL}^{2+}$. The inset shows the $\mathbf{CoL}^{+}$ formation kinetics recorded at 680 nm under the same conditions with 500 μM $\mathbf{CoL}^{2+}$. (b) Kinetic traces recorded at 678 nm following pulse radiolysis of 1.28 mM solutions of $\mathbf{CoL}^{2+}$ in Ar-purged (upper, black) and N_2O-saturated (lower, blue) CH_3CN. The red curves give fits to second-order (1.2×10^{10} M^{-1} s^{-1}, upper,) and biexponential (3.9×10^4 s^{-1} and 3.7×10^3 s^{-1}, lower) kinetic models. The inset shows representative radiation dose dependencies of $G(\mathbf{CoL}^{+})$ values measured in Ar-purged solutions with various

concentrations of $\mathbf{CoL^{2+}}$. From bottom to top: [$\mathbf{CoL^{2+}}$] = 0.029, 0.30, 2.6, and 25 mM. Each data point and error bars represent averages and standard deviations, respectively, for 5–10 individual measurements, and the lines give the linear fits.

To evaluate the radiation yields of $\mathbf{CoL^{+}}$, multiple traces of $\mathbf{CoL^{+}}$ decay at various $\mathbf{CoL^{2+}}$ concentrations and radiation doses were collected, fitted to second-order decays, and the fitted initial absorption values along with the dosimetry data and known $\mathbf{CoL^{+}}$ molar absorption coefficient[36] were used to calculate $G(\mathbf{CoL^{+}})$. As seen in Figure 2b, inset, these values depend not only on [$\mathbf{CoL^{2+}}$], which is expected, but also somewhat decrease with the radiation dose due to the competition between reaction 5 and e^-_{solv} scavenging by other radiolysis products, most notably with H^+_{solv}. To minimize this effect, the dose dependencies were linearly extrapolated to zero dose and the resulting $G(\mathbf{CoL^{+}})$ are plotted in Figure 3.

Based on the $\mathbf{CoL^{2+}}$ electron scavenging rate constant (k_5) and the natural lifetime of e^-_{solv} (Figure 2a), one would expect ~99% scavenging of e^-_{solv} and, hence, saturation of the $G(\mathbf{CoL^{+}})$ vs [$\mathbf{CoL^{2+}}$] dependence at ~0.6 mM $\mathbf{CoL^{2+}}$, when the scavenging time $\tau_s = 1/(k_5[\mathbf{CoL^{2+}}]) \approx 10$ ns becomes much shorter than the e^-_{solv} natural decay half-time of ~500 ns. However, as seen in Figure 3, saturation is not observed, and $G(\mathbf{CoL^{+}})$ continues to increase, reaching 2.8 ± 0.2 at [$\mathbf{CoL^{2+}}$] = 220 mM, the highest attainable concentration. The shape of the $G(\mathbf{CoL^{+}})$ vs [$\mathbf{CoL^{2+}}$] curve indicates that at the higher $\mathbf{CoL^{2+}}$ concentrations, there is a substantial contribution to the observed $G(\mathbf{CoL^{+}})$ from the scavenging of electrons that in the absence of a scavenger, recombine with other solvent radiation products on a shorter timescale than the 2–3 ns response time of our apparatus, which includes geminate and intraspur recombination. (In pulse radiolysis, spurs are well-separated nanoscale volumes containing several solvated electrons and other reactive species created along

the track of a high-energy electron passing through a liquid.) This assertion is supported by a decrease of the e^-_{solv} absorption amplitude with an increase of [$\mathbf{CoL^{2+}}$], notable in Figure 2a.

The magnitude of $G(\mathbf{CoL^{+}})$ at the highest point in Figure 3 gives a lower limit of 2.8 per 100 eV for the prompt radiation yield of e^-_{solv} in liquid CH_3CN (the solvent ionization yield) for low linear energy transfer radiation (gamma rays and relativistic electrons). Most likely, the actual yield is much larger than this limit, possibly close to or larger than the prompt solvated electron yield of 4.2 per 100 eV that has been observed in liquid water.[39] Indeed, the gas phase ionization energy of CH_3CN (12.20 eV) is somewhat lower than that of H_2O (12.62 eV).[40]

All previously reported solvated electron yields in CH_3CN, which average to 1.5 ± 0.4 per 100 eV (Table S1), were deduced from scavenging experiments. These yields vary widely and are lower than the yields observed in this study at [$\mathbf{CoL^{2+}}$] > 8 mM (Figure 3). Factors that may account for these variances include: (i) the electron scavenging rate constant and the maximum concentration of scavenger employed, the product of which is referred to as the scavenging power, (ii) the accuracy with which the molar absorption coefficient of the one-electron reduced scavenger product, ε_{scav}, is known, (iii) the solvent purity with respect to the contaminants reactive toward e^-_{solv} that accelerate its natural decay, and (iv) the radiation doses used. The lower values of the electron yield in SI Table S1 are likely due to the use of scavenging systems with lower scavenging power than were used in our experiments, together with the fact that in most cases, the ε_{scav} values were obtained from transient spectroscopy measurements in solvents other than CH_3CN, which may lead to errors in the solvated electron yields.[8]

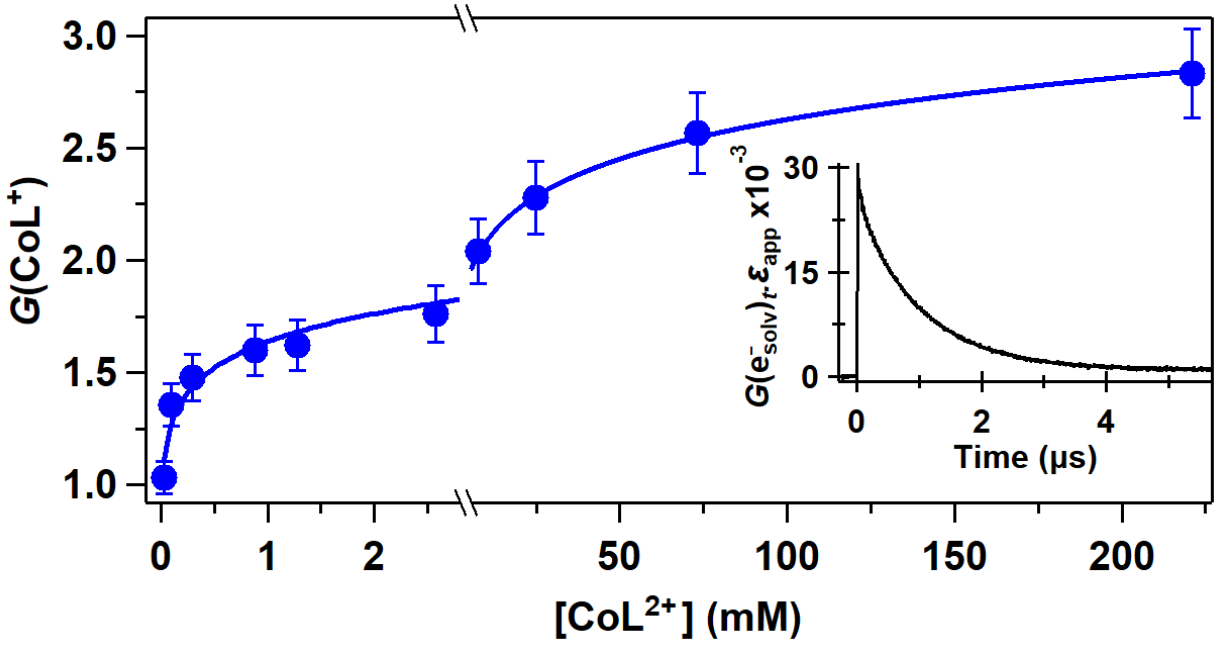

Figure 3. The concentration dependence of the observed $G(\mathbf{CoL}^{+})$ in Ar-purged CH_3CN. The smooth curve serves as a visual aid only. These data are also tabulated in SI Table S2. The inset shows a time dependence of $G(e^-_{solv})_t\varepsilon_{app}$ (in units of ions (100 eV)$^{-1}$ M^{-1} cm^{-1}), obtained from a 1450 nm transient absorption kinetic trace of e^-_{solv} decay in N_2-purged CH_3CN at 20 °C and thiocyanate dosimetry data (SI Figure S6a gives a more detailed view of this kinetic trace).

Molar absorption coefficients and spectra. From e^-_{solv} absorption decay at 1450 nm in conjunction with dosimetry, we have evaluated the time-dependent $G(e^-_{solv})_t\varepsilon_{app}$ product, where $G(e^-_{solv})_t$ is the apparent time-dependent solvated electron yield, and ε_{app} is the weighted average of the molar absorption coefficients of e^-_{cav} and $(CH_3CN)_2^{\bullet-}$ at this wavelength,

$$\varepsilon_{app} = \frac{\varepsilon_{cav} + \varepsilon_{dsa}K^o}{1+K^o} \qquad (8)$$

The resulting $G(e^-_{solv})_t\varepsilon_{app}$ kinetics is plotted in Figure 3, inset. This kinetics is related to the measured $G(\mathbf{CoL}^+)$ values through a Laplace transform; that is,

$$G(\mathbf{CoL}^+) = \frac{k_5[\mathbf{CoL}^{2+}]}{\varepsilon_{app}} \int_0^\infty G(e^-_{solv})_t \varepsilon_{app} \exp\left(-k_5[\mathbf{CoL}^{2+}]t\right) dt \qquad (9)$$

We have resorted to a Laplace transform only because the e^-_{solv} decay could not be satisfactorily described by an exponential function (Figure S1) and the use of a simpler kinetic model for correlating $G(\mathbf{CoL}^+)$ with $G(e^-_{solv})$ based on a competition between the pseudo first-order electron scavenging and its first-order decay, as was done by Rodgers and co-workers,[5] would be inadequate.

For evaluating ε_{app}, integration in eq. 9 must be applied over the time range in which the $G(e^-_{solv})_t\varepsilon_{app}$ product is known (i.e., from 2–3 ns after the radiation pulse) and with the $G(\mathbf{CoL}^+)$ values measured when virtually all scavenging occurs within this time range. Based on these considerations, a $\mathbf{CoL}^{2+}$ concentration of 29 μM, for which $G(\mathbf{CoL}^+) = 1.03 \pm 0.07$ per 100 eV (the leftmost point in Figure 3), has been chosen for evaluating ε_{app} through eq. 9. At this concentration, the scavenging time, $\tau_s \approx 220$ ns is significantly shorter than the natural decay time of the solvated electrons but long enough to exclude e^-_{solv} scavenging during the response time of our detection system used for measuring the $G(e^-_{solv})_t\varepsilon_{app}$ kinetics. Indeed, a comparison of the red and black curves in Figure 2a shows that even at the higher $\mathbf{CoL}^{2+}$ concentration of 49 μM, there is virtually no decrease in the initial amplitude of the e^-_{solv} absorption.

Application of the chosen $\mathbf{CoL}^{2+}$ concentration and $G(\mathbf{CoL}^+)$ yields $\varepsilon_{app} = (20.8 \pm 1.5) \times 10^3$ M^{-1} cm^{-1} at 1450 nm (see SI Section 7 for details of this procedure). Using this value in eq. 8, along with $K° = 0.60 \pm 0.49$ at 20 °C and $\varepsilon_{cav}/\varepsilon_{dsa} = 24.5 \pm 5.1$ at 1450 nm that have been previously determined in this study, we obtain $\varepsilon_{dsa} = (1.3 \pm 0.5) \times 10^3$ and $\varepsilon_{cav} = (32.4 \pm 9.6) \times 10^3$ M^{-1} cm^{-1}

at this wavelength. The large uncertainties in these values almost entirely arise from the substantial uncertainty in $K°$, the origin of which was discussed earlier. On the other hand, the ε_{app} uncertainty is relatively much smaller, and in practice, this parameter is more consequential because it allows direct quantitative evaluation of the solvated electron concentrations from its transient absorption amplitude in pulse radiolysis or flash photolysis experiments.

In their pioneering paper, Rodgers and co-workers used pyrene and stilbene as the electron scavengers to derive a molar absorption coefficient of 23×10^3 M^{-1} cm^{-1} at 1450 nm for the high-temperature solvated electron state,[5] which we now understand to be e^-_{cav}. However, a careful reading reveals that this value actually represents ε_{app} rather than ε_{cav} and, as such, agrees well with our ε_{app} value. Moreover, Rodgers and co-workers could not possibly determine the individual molar absorption coefficients of the two solvated electron species because it would require a knowledge of $K°$ (eq. 8), which had not been evaluated in their work. When deriving the equilibrium constant for reaction 1 and spectra of e^-_{cav} and $(CH_3CN)_2^{\bullet-}$,[28] Doan and Schwartz used the Rodgers and co-workers' molar absorption coefficient without realizing that it was misassigned, which undoubtedly contributed to their overestimation of $K°$ and underestimation of ε_{cav} and ε_{dsa}.

The absorption spectra of e^-_{cav} and $(CH_3CN)_2^{\bullet-}$, have been reconstructed from two transient absorption spectra of e^-_{solv} recorded at widely different temperatures, namely 233 and 348 K, values of $K°$ at these temperatures (Figure 1b), and our $\varepsilon_{cav} = (32.4 \pm 9.6) \times 10^3$ M^{-1} cm^{-1} at 1450 nm (for details, see SI Section 8). The resulting spectra are shown in Figure 4, where the relatively large error bars arise from the substantial uncertainties in $K°$, which was discussed earlier (Figure 1b). As a reality check, it is instructive to estimate the oscillator strength of the cavity electron absorption band, $f(e^-_{cav})$. Using the e^-_{cav} spectrum in Figure 4 and a procedure described by Bartels

and co-workers,[41] we have estimated $f(e^-_{cav}) = 0.91 \pm 0.28$ (see SI Section 9 for details). Although quite approximate, this value is comfortably close to unity, as is the case for the solvated electron in other polar solvents.[42, 41]

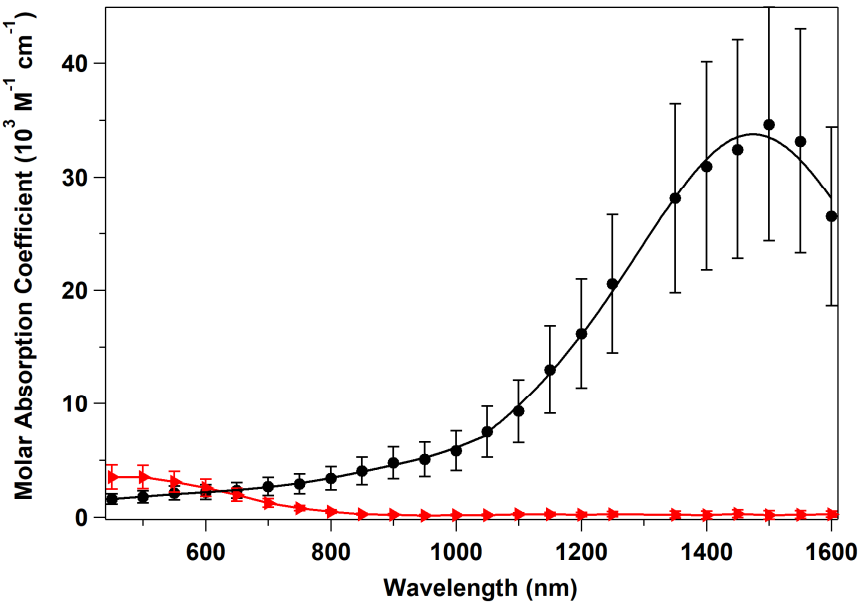

Figure 4. Absorption spectra of e^-_{cav} (black circles) and $(CH_3CN)_2^{\bullet-}$ (red triangles), reconstructed by applying a procedure described in the SI Section 8 to transient absorption spectra recorded following pulse radiolysis of neat N_2-purged CH_3CN at 233 and 348 K.

CONCLUSIONS

Previous studies have established that the solvated electrons, e^-_{solv}, in liquid acetonitrile occupy two structurally distinct states that are in rapid equilibrium with each other, namely, a solvent cavity-localized electron, e^-_{cav}, and a dimeric solvent anion radical, $(CH_3CN)_2^{\bullet-}$ (so that $[e^-_{solv}] = [e^-_{cav}] + [(CH_3CN)_2^{\bullet-}]$). Whereas the former exhibits a strong NIR band around 1450 nm, the latter only weakly absorbs in the UV-Vis. The literature data on the equilibrium between e^-_{cav} and $(CH_3CN)_2^{\bullet-}$ differ substantially. In the present work, we have used pulse radiolysis in the 233-353

K temperature range to obtain the equilibrium standard enthalpy $\Delta H° = -11.2 \pm 0.3$ kcal/mol and entropy $\Delta S° = -39.3 \pm 1.2$ cal/(mol K). These values correspond to an equilibrium constant of $K° = 0.44 \pm 0.35$ at 25 °C, which indicates a predominance of the e^-_{cav} state near and above this temperature and revises the most recently reported room temperature $K°$ of 4.1 ± 0.2. Variances between ours and other pertinent previously reported thermochemical data are extensively discussed.

Presently, acetonitrile is the only solvent in which an equilibrium between two metastable solvated electron states that strongly shifts from one state to the other with temperature has been observed. A thermochemical analysis shows that: (i) in order to observe such a shift, the equilibrium values of $\Delta H°$ and $\Delta S°$ must reside within a small cuneate area on the $\Delta H°$-$\Delta S°$ surface, and (ii) the uniqueness of CH_3CN arises mainly from a serendipitous alignment of these parameters, and the chances of discovering a similar equilibrium in another solvent are small.

To quantify the radiation chemical yield of the solvated electrons, we employed a Co(II) cyclam macrocycle (**CoL**$^{2+}$, Scheme 1a) that captures e^-_{solv} with a rate constant of $(1.55 \pm 0.02) \times 10^{11}$ M^{-1} s^{-1} (Scheme 1b) to produce a long-lived **CoL**$^+$ species, which exhibits a strong characteristic absorption band at 680 nm with an accurately known molar absorption coefficient in CH_3CN. In N_2O-saturated CH_3CN, the **CoL**$^+$ production is efficiently suppressed due to competitive e^-_{solv} scavenging by N_2O that occurs with a $(6.42 \pm 0.06) \times 10^9$ atm^{-1} s^{-1} rate constant.

The apparent e^-_{solv} radiation yield, $G(e^-_{solv})$, monotonically increases without saturation over the entire attainable scavenger concentration range, reaching 2.8 per 100 eV at [**CoL**$^{2+}$] = 0.220 M. This value represents the lower limit for acetonitrile ionization in pulse radiolysis and is substantially larger than all previous $G(e^-_{solv})$ estimates ranging from 1.01–2.03 per 100 eV. The

actual CH_3CN ionization yield is likely to be substantially larger than our limiting value, possibly close to the water ionization yield that exceeds 4 per 100 eV.

The apparent molar absorption coefficient, $\varepsilon_{app} = (20.8 \pm 1.5) \times 10^3$ M^{-1} cm^{-1} at 1450 nm and 20 °C, for the solvated electrons was derived from an analysis of their time-dependent yield. From the scavenging data and measurements of transient e^-_{solv} spectra at 233 and 348 K, the individual Vis-NIR absorption spectra of e^-_{cav} and $(CH_3CN)_2^{\bullet-}$ have been reconstructed, the molar absorption coefficient of e^-_{cav} determined to be $(32.4 \pm 9.6) \times 10^3$ M^{-1} cm^{-1} at 1450 nm, and the oscillator strength for the NIR absorption band of e^-_{cav} estimated as 0.91 ± 0.28, which is in line with the oscillator strengths for the solvated electron absorption bands in other polar solvents.[42, 41]

In summary, the present investigation serves to resolve several controversies concerning the solvated electron properties in CH_3CN, which, together with the newly obtained data, will facilitate quantitative pulse radiolysis investigations in this commonly used solvent.

ASSOCIATED CONTENT

Supporting Information

The Supporting Information is available free of charge at https://pubs.acs.org/doi/10.1021/……...

Additional experimental details, thermodynamic estimates and discussion of restrictions on $\Delta H°$ and $\Delta S°$ to observe equilibrium, discussion of the Bell, Rodgers and Burrows equilibrium analysis, comparison of reported vertical binding energies with our $\Delta H°$, $\mathbf{CoL^{2+}}$ and N_2O electron scavenging data, detailed procedures for the evaluation of molar absorption coefficients, reconstruction of the absorption spectra, and oscillator strength estimation, supporting tables (PDF)

AUTHOR INFORMATION

Corresponding Authors

David C. Grills – *Chemistry Division, Brookhaven National Laboratory, Upton, NY 11973-5000, United States*; orcid.org/0000-0001-8349-9158; Email: dcgrills@bnl.gov

Sergei V. Lymar – *Chemistry Division, Brookhaven National Laboratory, Upton, NY 11973-5000, United States*; orcid.org/0000-0003-2663-6157; Email: lymar@bnl.gov

Notes

The authors declare no competing financial interests.

ACKNOWLEDGMENT

This work and use of the Laser Electron Accelerator Facility and Van de Graaff facilities of the Accelerator Center for Energy Research at BNL, was supported by the U.S. Department of Energy (DOE), Office of Science, Office of Basic Energy Sciences, Division of Chemical Sciences, Geosciences & Biosciences under contract DE-SC0012704. We thank Dr. Etsuko Fujita for the synthesis of *N-rac*-[Co(HMD)(H_2O)](ClO_4)$_2$.

REFERENCES

(1) Singh, A.; Gesser, H. D.; Scott, A. R. Solvated Electron in Acetonitrile. *Chem. Phys. Lett.* **1968,** *2*, 271-273.
(2) Hayon, E. Yield of Ions and Excited States Produced in the Radiolysis of Polar Organic Liquids. *J. Chem. Phys.* **1970,** *53*, 2353-2358.
(3) Baptista, J. L.; Burrows, H. D. Solute Ion and Radical Formation in the Pulse Radiolysis of Acetonitrile Solutions. *J. Chem. Soc., Faraday Trans. 1* **1974,** *70*, 2066-2079.
(4) Burrows, H. D.; Kosower, E. M. Optical Spectra and Reactivities of Radical Anions of 4-Nitrobenzyl Compounds Produced by Pulse Radiolysis of Acetonitrile Solutions. *J. Phys. Chem.* **1974,** *78*, 112-117.
(5) Bell, I. P.; Rodgers, M. A. J.; Burrows, H. D. Kinetic and Thermodynamic Character of Reducing Species Produced on Pulse Radiolysis of Acetonitrile. *J. Chem. Soc., Faraday Trans. 1* **1977,** *73*, 315-326.
(6) Bobrowski, K.; Das, P. K. Transient Phenomena in the Pulse Radiolysis of Retinyl Polyenes. 4. Environmental Effects on Absorption Maximum of Retinal Radical Anion. *J. Phys. Chem.* **1985,** *89*, 5733-5738.
(7) Nakayama, T.; Ushida, K.; Hamanoue, K.; Washio, M.; Tagawa, S.; Tabata, Y. Pulse Radiolyses of Anthraquinone and Anthraquinone-Triethylamine in Acetonitrile and Toluene at Room Temperature. *J. Chem. Soc., Faraday Trans.* **1990,** *86*, 95-103.
(8) Imamura, T.; Sumiyoshi, T.; Takahashi, K.; Sasaki, Y. Radiolytic Studies of Ruthenium Oxo-Acetato Trinuclear Complexes in Acetonitrile. *J. Phys. Chem.* **1993,** *97*, 7786-7791.
(9) Nad, S.; Pal, H. Photoinduced Electron Transfer from Aliphatic Amines to Coumarin Dyes. *J. Chem. Phys.* **2002,** *116*, 1658-1670.
(10) De la Fuente, J. R.; Kciuk, G.; Sobarzo-Sanchez, E.; Bobrowski, K. Transient Phenomena in the Pulse Radiolysis of Oxoisoaporphine Derivatives in Acetonitrile. *J. Phys. Chem. A* **2008,** *112*, 10168-10177.
(11) Grills, D. C.; Farrington, J. A.; Layne, B. H.; Lymar, S. V.; Mello, B. A.; Preses, J. M.; Wishart, J. F. Mechanism of the Formation of a Mn-Based CO_2 Reduction Catalyst Revealed by Pulse Radiolysis with Time-Resolved Infrared Detection. *J. Am. Chem. Soc.* **2014,** *136*, 5563-5566.
(12) Grills, D. C.; Lymar, S. V. Radiolytic Formation of the Carbon Dioxide Radical Anion In Acetonitrile Revealed by Transient IR Spectroscopy. *Phys. Chem. Chem. Phys.* **2018,** *20*, 10011-10017.
(13) Skotnicki, K.; De la Fuente, J. R.; Canete, A.; Berrios, E.; Bobrowski, K. Radical Ions of 3-Styryl-quinoxalin-2-one Derivatives Studied by Pulse Radiolysis in Organic Solvents. *J. Phys. Chem. B* **2018,** *122*, 4051-4066.
(14) Xia, C. G.; Peon, J.; Kohler, B. Femtosecond Electron Ejection in Liquid Acetonitrile: Evidence for Cavity Electrons and Solvent Anions. *J. Chem. Phys.* **2002,** *117*, 8855-8866.
(15) Shkrob, I. A.; Sauer, M. C., Jr. Electron Localization in Liquid Acetonitrile. *J. Phys. Chem. A* **2002,** *106*, 9120-9131.
(16) Belloni, J.; Marignier, J.-L. Electron-Solvent Interaction: Attachment Solvation Competition. *Radiat. Phys. Chem.* **1989,** *34*, 157-171.
(17) Shkrob, I. A.; Takeda, K.; Williams, F. Electron Localization in Solid Acetonitrile. *J. Phys. Chem. A* **2002,** *106*, 9132-9144.

(18) Mitsui, M.; Ando, N.; Kokubo, S.; Nakajima, A.; Kaya, K. Coexistence of Solvated Electrons and Solvent Valence Anions in Negatively Charged Acetonitrile Clusters, $(CH_3CN)_n^-$ (n = 10-100). *Phys. Rev. Lett.* **2003,** *91*, 153002.
(19) Young, R. M.; Griffin, G. B.; Kammrath, A.; Ehrler, O. T.; Neumark, D. M. Time-Resolved Dynamics in Acetonitrile Cluster Anions $(CH_3CN)_n^-$. *Chem. Phys. Lett.* **2010,** *485*, 59-63.
(20) Shreve, A. T.; Elkins, M. H.; Neumark, D. M. Photoelectron Spectroscopy of Solvated Electrons in Alcohol and Acetonitrile Microjets. *Chem. Sci.* **2013,** *4*, 1633-1639.
(21) Takayanagi, T. Theoretical Simulations of Dynamics of Excess Electron Attachment to Acetonitrile Clusters. *Chem. Phys.* **2004,** *302*, 85-93.
(22) Takayanagi, T. *Ab Initio* Study of Small Acetonitrile Cluster Anions. *J. Chem. Phys.* **2005,** *122*, 244307.
(23) Takayanagi, T.; Hoshino, T.; Takahashi, K. Electronic Structure Calculations of Acetonitrile Cluster Anions: Stabilization Mechanism of Molecular Radical Anions by Solvation. *Chem. Phys.* **2006,** *324*, 679-688.
(24) Timerghazin, Q. K.; Peslherbe, G. H. Electronic Structure of the Acetonitrile and Acetonitrile Dimer Anions: A Topological Investigation. *J. Phys. Chem. B* **2008,** *112*, 520-528.
(25) Azar, J.; Kurlancheek, W.; Head-Gordon, M. Characterization of Electronically Excited States in Anionic Acetonitrile Clusters. *Phys. Chem. Chem. Phys.* **2011,** *13*, 9147-9154.
(26) Narvaez, W. A.; Schwartz, B. J. *Ab Initio* Simulations of Poorly and Well Equilibrated $(CH_3CN)_n^-$ Cluster Anions: Assigning Experimental Photoelectron Peaks to Surface-Bound Electrons and Solvated Monomer and Dimer Anions. *J. Phys. Chem. A* **2021,** *125*, 7685-7693.
(27) Equation 2 implies a pure liquid standard sate with activity of unity for CH_3CN and 1 mole/L standard states for $[e_{cav}^-]$ and $(CH_3CN)_2^{\bullet-}$.
(28) Doan, S. C.; Schwartz, B. J. Ultrafast Studies of Excess Electrons in Liquid Acetonitrile: Revisiting the Solvated Electron/Solvent Dimer Anion Equilibrium. *J. Phys. Chem. B* **2013,** *117*, 4216-4221.
(29) Doan, S. C.; Schwartz, B. J. Nature of Excess Electrons in Polar Fluids: Anion-Solvated Electron Equilibrium and Polarized Hole-Burning in Liquid Acetonitrile. *J. Phys. Chem. Lett.* **2013,** *4*, 1471-1476.
(30) Samant, V.; Singh, A. K.; Mukherjee, T.; Palit, D. K. Spectroscopic Properties of Anion Radicals Studied Using Pulse Radiolysis. *Res. Chem. Intermed.* **2006,** *32*, 767-776.
(31) Szalda, D. J.; Schwarz, C. L.; Endicott, J. F.; Fujita, E.; Creutz, C. Solution Studies Of The Cobalt(II) *N-rac* and *N-meso*-CoL^{2+} Isomers and Molecular and Crystal Structures of the Low-Spin, Five-Coordinate Cobalt(II) Macrocyclic Complexes *N-rac*-$[CoL(H_2O)](ClO_4)_2 \bullet 0.6H_2O$ (1) and *N-rac*-$[CoL(OClO_3]ClO_4$ (2) (L = 5,7,7,12,14,14-Hexamethyl-1,4,8,11-tetraazacyclotetradeca-4,11-diene). *Inorg. Chem.* **1989,** *28*, 3214-3219.
(32) Wishart, J. F.; Cook, A. R.; Miller, J. R. The LEAF Picosecond Pulse Radiolysis Facility at Brookhaven National Laboratory. *Rev. Sci. Instrum.* **2004,** *75*, 4359-4366.
(33) Itoh, K.; Holroyd, R. Effect of Pressure on The Electron Mobility in Liquid Benzene and Toluene. *J. Phys. Chem.* **1990,** *94*, 8850-8854.
(34) Tran-Thi, T. H.; Koulkès-Pujo, A. M. Electron Attachment to Amides Studied by Low-Pressure Chemical Ionization And Electron Swarms - Comparison of the Gas and Liquid Phase. *Can. J. Phys.* **1985,** *63*, 560-566.

(35) Shkrob, I. A.; Sauer, M. C., Jr. Radical Ions in Liquids. In *Charged Particle and Photon Interactions with Matter*, 1st ed.; Mozumder, A.; Hatano, Y., Eds. CRC Press: Boca Raton, 2003; pp 301-330.
(36) Fujita, E.; Szalda, D. J.; Creutz, C.; Sutin, N. Carbon Dioxide Activation: Thermodynamics of CO_2 Binding and the Involvement of Two Cobalt Centers in the Reduction of CO_2 by a Cobalt(I) Macrocycle. *J. Am. Chem. Soc.* **1988,** *110*, 4870-4871.
(37) Creutz, C.; Schwarz, H. A.; Wishart, J. F.; Fujita, E.; Sutin, N. Thermodynamics and Kinetics of Carbon Dioxide Binding to Two Stereoisomers of a Cobalt(I) Macrocycle in Aqueous Solution. *J. Am. Chem. Soc.* **1991,** *113*, 3361-3371.
(38) Tait, A. M.; Hoffman, M. Z.; Hayon, E. The Reactivity of Cobalt(I) Complexes Containing Unsaturated Macrocyclic Ligands in Aqueous Solution. *J. Am. Chem. Soc.* **1976,** *98*, 86-93.
(39) Wang, F. R.; Schmidhammer, U.; Larbre, J. P.; Zong, Z. Z.; Marignier, J.-L.; Mostafavi, M. Time-Dependent Yield of the Hydrated Electron and the Hydroxyl Radical in D_2O: A Picosecond Pulse Radiolysis Study. *Phys. Chem. Chem. Phys.* **2018,** *20*, 15671-15679.
(40) Lias, S. G. Ionization Energy Evaluation. In *NIST Chemistry WebBook, NIST Standard Reference Database Number 69*, Linstrom, P. J.; Mallard, W. G., Eds. National Institute of Standards and Technology, Gaithersburg MD, 20899, https://doi.org/10.18434/T4D303, (retrieved August 13, 2021).
(41) Hare, P. M.; Price, E. A.; Stanisky, C. M.; Janik, I.; Bartels, D. M. Solvated Electron Extinction Coefficient and Oscillator Strength in High Temperature Water. *J. Phys. Chem. A* **2010,** *114*, 1766-1775.
(42) Jou, F. Y.; Freeman, G. R. Shapes of Optical Spectra of Solvated Electrons. Effect of Pressure. *J. Phys. Chem.* **1977,** *81*, 909-915.

TOC Graphic